*Acta Oceanol. Sin.*, 2021, Vol. 40, No. 11, P. 129–137
https://doi.org/10.1007/s13131-021-1760-z
http://www.aosocean.com
E-mail: ocean2@hyxb.org.cn

# Wave-ice dynamical interaction: a numerical model and its application

Yang Zhang[1]*, Changsheng Chen[2], Guoping Gao[3], Jianhua Qi[2], Huichan Lin[2], Wei Yu[4], Liang Chang[4]

[1] State Key Laboratory of Satellite Ocean Environment Dynamics, Second Institute of Oceanography, Ministry of Natural Resources, Hangzhou 310012, China

[2] School for Marine Science and Technology, University of Massachusetts-Dartmouth, New Bedford MA 02744-1221, USA

[3] College of Marine Ecology and Enviroment, Shanghai Ocean University, Shanghai 201306, China

[4] College of Marine Sciences, Shanghai Ocean University, Shanghai 201306, China

Received 5 December 2020; accepted 20 December 2020



**Abstract**

In this paper, an ice floe inner stress caused by the wave-induced bending moment is derived to estimate the stress failure of ice floe. The strain and stress failures are combined to establish a wave-induced ice yield scheme. We added ice stress and strain failure module in the Finite-Volume Community Ocean Model (FVCOM), which already includes module of ice-induced wave attenuation. Thus a fully coupled wave-ice dynamical interaction model is established based on the ice and wave modules of FVCOM. This model is applied to reproduce the ice and wave fields of the breakup events observed during the second Sea Ice Physics and Ecosystem Experiment (SIPEX-2) voyage. The simulation results show that by adopting the combined wave-induced ice yield scheme, the model can successfully predict the ice breakup events, which the strain failure model is unable to predict. By comparing the critical significant wave height deduced from strain and stress failure schemes, it is concluded that the ice breakup is caused by the strain failure when wave periods are shorter than a threshold value, while the stress failure is the main reason for the ice breakup when wave periods are longer than the threshold value. Neglecting either of these two ice-break inducement mechanisms could overestimate the ice floe size, and thus underestimate the velocity of the ice lateral melt and increase the error of simulation of polar ice extent.

**Key words:** wave-ice interaction, FVCOM, stress failure, ice lateral melt

**Citation:** Zhang Yang, Chen Changsheng, Gao Guoping, Qi Jianhua, Lin Huichan, Yu Wei, Chang Liang. 2021. Wave-ice dynamical interaction: a numerical model and its application. Acta Oceanologica Sinica, 40(11): 129–137, doi: 10.1007/s13131-021-1760-z

## 1 Introduction

Since the latter half of the 20th century, due to global warming, the Arctic sea ice has thinned, which is a threat against the sea state and atmospheric forcing. The indication is embodied in two aspects: the persistently and rapidly receding summer ice extent ($3.8\times10^5$ km$^2$ per decade) (Cavalieri et al., 2003; Meier et al., 2005), and the decrease of the multi-year sea ice thickness (e.g. about 0.6 m from 2003 to 2008) (Kwok et al., 2009). Meanwhile, the climate model results did not appropriately match with the updated changes of the ice in the Arctic region (Stroeve et al., 2007). In a recent research, the ice-wave interaction was suggested to be taken into consideration in order to improve the accuracy of thermodynamic models so that this problem may be solved (Kohout et al., 2014; Squire, 2020).

Field observations (Robin, 1963; Dean, 1966; Wadhams et al., 1988; Liu et al., 1991; Doble and Bidlot, 2013; Kohout et al., 2014) showed that the waves can propagate into the marginal ice zone (MIZ) and this energy is gradually attenuated by ice floes. In addition, the attenuation rate is sensitively controlled by the peak period of waves and the ice property, including the ice concentration, the ice thickness, and the ice floe diameter. Squire and Meylan (1994) and Squire (2007, 2020) systematically and comprehensively summarized previous works on the ice-wave interaction. Among many ice-induced wave attenuation models, one commonly recognized and practical branch treated the ice field as a mass of individual ice floes with the inclusion of the wave energy attenuation, reflection, and transmission using a scattering-method formulation (Kohout and Meylan, 2008; Squire et al., 2009; Doble and Bidlot, 2013; Kohout et al., 2014). Kohout and Meylan (2008), focusing on the wave attenuation in the MIZ, proposed an ice-induced wave attenuation model for waves with periods in the range of 6–16 s. As the energy of waves with longer periods can penetrate deep into the Arctic sea, Squire et al. (2009) proposed an ice-induced wave attenuation coefficient formulation for waves with periods longer than 10 s. This coefficient allows a more versatile wave model to be implemented for more general cases, in which waves with longer periods penetrate into the ice-covered Arctic waters beyond the MIZ. Zhang et al.

Foundation item: The National Natural Science Foundation of China under contract Nos 41606208 and 41276197; the National Natural Science Foundation of USA under contract Nos OCE-1203393, OCE-109341 and PLR-1603000; the Global Change Research Program of China under contract No. 2015CB953900; the Shanghai Eastern Scholar Program under contract No. 2012-58; the Project of State Key Laboratory of Satellite Ocean Environment Dynamics, Second Institute of Oceanography under contract No. SOEDZZ1805.

*Corresponding author, E-mail: yzhang@sio.org.cn

(2020), by combining the former two models (Kohout and Meylan, 2008; Squire et al., 2009), suggested an ice-induced wave attenuation parameterization method to form a more practical method for basin-scale numerical wave models. The work of Zhang et al. (2020) was not only for the purpose of simulation of the wave energy decay in the MIZ but also aimed at estimation of the wave energy in the deep ice-covered sea and the wave field in the whole Arctic basin. Recently, Bai et al. (2020) developed a partly coupled wave-ice model based on FVCOM and the ice-induced wave attenuation scheme from WAVEWATCH III® IC4. This model has been used to study the wave field evolution in the Great Lakes and has been adopted by Fujisaki-Manome et al. (2020) for relevant research.

Along with the ice-induced wave attenuation, waves can influence the ice thermodynamics by enlarging the ice surface due to the wave-induced ice floe breakup. For instance, the intrusion of swells in the Beaufort Sea was observed (Asplin et al., 2012), which propagated approximately 250 km into the multi-year pack ice and broke the ice floes. This process enlarged the ice surface and could accelerate the ice melting rate by increasing the ice-air and ice-water thermal interactions. The elastic plate theory is an approach to estimate the wave-induced ice breakup. This theory treats the ice plate as a flexible material with limited rigidity and assumes the ice floe is broken because of strain failure (Williams et al., 2013a, b). Dumont et al. (2011) analyzed two extreme approaches to measure bending failure. One approach treats the ice floe as an elastic plate and links the ice breakup to the wave-induced flexural strain, which exceeds the critical strain. This approach and the theory raised by Williams et al. (2013a, b) are appropriate for the MIZ, where sizes of the ice floes, both thickness and diameter, are small and the ice strength is weak. Kohout et al. (2015) collected the observed wave data during the second Sea Ice Physics and Ecosystem Experiment (SIPEX-2) voyage when three ice floe breakup events occurred in the Aurora Australia. Kohout et al. (2015) considered ice floes as elastic plates and the breakup happened because of the over-threshold strain. However, two of the three observed significant wave heights, which indeed caused the ice breakup, were lower than the critical significant wave height derived from the theory of strain failure. Thus, the strain failure theory may not fully resolve the ice floe breakup event. Based on the theory of Kohout et al. (2015), the strain within the floe ($E_s$) was related to the wave height ($h$), the ice thickness ($H$), and the peak period ($T$) as follows:

$$E_s \sim hHT^{-4}. \tag{1}$$

Equation (1) implies that thicker ice floes cause higher strains, but it is not reasonable because the ice floe is not an ideal elastic material as it is partially rigid. Equation (1) also shows that higher wave peak periods result in lower strains, which make the ice floe less probable to break up. In contrast, two of three ice floe breakup events, observed during the SIPEX-2 voyage in the Aurora Australia, occurred when wave peak periods were about 15 s and the significant wave heights were only about 0.1 m.

The other approach of Dumont et al. (2011) treats the ice floe as a rigid material, and the ice floe is assumed to break due to the stress failure. Note that this approach was designed to resolve the ice breakup due to the effects of long waves. However, Dumont et al. (2011) did not provide a clear discussion of the stress failure inducing the ice breakup. In addition, Dumont et al. (2011) introduced Eq. (2) for the flexural stress in the ice floe when a wave was traveling through.

$$\sigma = \frac{3g\overline{\rho}A\lambda^2}{2\pi h^2}, \tag{2}$$

where $g$ is the acceleration of gravity, $\overline{\rho}$ is the mean density of sea water and ice, $A$ is the wave amplitude, $\lambda$ is wave length; and $h$ is the ice floe thickness.

Equation (2) was derived based on the flexural stress suggested by Schwarz et al. (1981) as Eq. (3),

$$\sigma = \frac{3FL}{2bh^2}, \tag{3}$$

where a single force ($F$) was applied on the ice floe. The length, height and width of the ice floe are $L$, $h$ and $b$ respectively. However, in reality the vertical forces exerting on the ice floe are the integration of pressure distributions imposed by passing waves.

Thus, in order to improve the wave-induced ice breakup parameterization, a statics theory based on the flexural stress model will be proposed in this study. Combining with the pre-validated ice-induced wave attenuation model and the strain failure model provided by Zhang et al. (2020), a wave-ice dynamical interaction model will be established, to explain the ice floe breakup events during the SIPEX-2 voyage. This paper is organized as follows. In Section 2, the wave-ice interaction model will be described, emphasizing the flexural stress model. In Section 3, the critical wave amplitude will be given and the ice floe breakup events during the SIPEX-2 voyage will be reproduced by the model, and the conclusions will be provided in Section 4.

## 2 Model description

### 2.1 *The wave-ice interaction model*

The proposed wave-ice interaction model is established based on the unstructured-grid Finite-Volume Community Ocean Model (FVCOM), which was developed by a joint research team at the University of Massachusetts-Dartmouth (UMASSD) and Woods Hole Oceanographic Institution (WHOI) (Chen et al., 2003, 2006, 2013). Two modules of FVCOM, unstructured-grid version of Simulating Wave Nearshore Model (called SWAVE) and Unstructured-Grid Community Ice CodE (UG-CICE), are included in this study, by which the sea surface wave and the ice property in the ocean, are simulated, respectively.

Note that FVCOM SWAVE is an unstructured-grid version of the Simulation Waves Nearshore (SWAN) originally developed by Qi et al. (2009) under the framework of FVCOM. The finite-volume advection scheme used in SWAVE performs with the same numerical accuracy as the third-order finite-difference method used in SWAN (Qi et al., 2009). In addition, the UG-CICE model is the unstructured-grid version of Community Ice CodE developed in the FVCOM group for studying the ice evolution and ice-ocean interaction. This model is fully coupled with unstructured Grid Global FVCOM (GB-FVCOM) through the exchange of heat, fresh/salt water, and momentum (Gao et al., 2011).

The interface of wave-ice dynamic interactions can be separately introduced as the ice-induced wave attenuation and the wave-induced ice floe breakup. The first part is adopted from Zhang et al. (2020) and will be introduced briefly. What we improved is the ice stress failure scheme. Based on the theory of Williams et al. (2013a) for the strain failure scheme, we added wave-induced ice floe breakup module in FVCOM.

### 2.2 *The ice-induced wave attenuation scheme*

In the Cartesian coordinate system, the wave growth, dissipation, and propagation are given by the governing equation of the wave action density spectrum balance as

$$\frac{\partial N}{\partial t}+\nabla\cdot\left[\left(\overrightarrow{C}_g+\overrightarrow{V}\right)N\right]+\frac{\partial C_\sigma N}{\partial\sigma}+\frac{\partial C_\theta N}{\partial\theta}=\frac{S_{\rm tot}}{\sigma}, \quad (4)$$

where $N$ is the wave action density spectrum, $\sigma$ is the relative frequency, $\theta$ is the wave direction, $C_\sigma$ and $C_\theta$ are the wave propagation velocities in the spectral space $(\sigma,\theta)$, $t$ is the time variable, the vector $\overrightarrow{C}_g$ is the wave group velocity, and the vector $\overrightarrow{V}$ is the ambient ocean current velocity (Zhang et al., 2020). In addition, $S_{\rm tot}$ is the source-sink term given as

$$S_{\rm tot}=S_{\rm in}+S_{\rm nl3}+S_{\rm nl4}+S_{\rm ds,w}+S_{\rm ds,b}+S_{\rm ds,br}+S_{\rm att,ice}, \quad (5)$$

where $S_{\rm in}$ is the wind energy input; $S_{\rm nl3}$ is the nonlinear transfer of the wave energy due to triadic three-wave interactions; $S_{\rm nl4}$ is the nonlinear transfer of the wave energy due to four-wave interactions; $S_{\rm ds,w}$, $S_{\rm ds,b}$, and $S_{\rm ds,br}$ are the three wave energy dissipation terms which represent the wave energy dissipation due to the whitecapping, the bottom friction, and the depth-induced wave breakup, respectively. The "blocking effect" for $S_{\rm in}$ is not considered in this paper, due to zero wind input in the ideal cases, which will be presented in Section 3.2. The "blocking effect" may influence other source-sink terms, i.e. $S_{\rm ds,w}$, but this work does not include it for the simplicity of the discussion.

The parameterization of $S_{\rm att,ice}$, which is the energy dissipation due to the ice-induced wave energy attenuation, is the same as Zhang et al. (2020) and FVCOM 4.0. Details of $S_{\rm att,ice}$ in the FVCOM can be found in Zhang et al. (2020).

### 2.3 *The wave-induced ice floe breakup*

In this study, the ice floe breakup is controlled by both the strain and stress failures because the ice is supposed neither an ideal elastic material nor a rigid body. Thus, both deformation and internal stress concentration can be a trigger of the ice breakup. Once the critical failure threshold is reached and half of the length of the dominating wave (of peak period) is shorter than the maximum of the ice floe size, the ice floe breakup is supposed to occur.

#### 2.3.1 *Strain failure*

To calculate the strain failure, the ice floe is treated as a thin elastic plate, and the passing wave is assumed to bend the ice floe, inducing strain in the ice. The significant strain amplitude $(E_{\rm s})$ of the ice floes is compared with the critical breaking strain $(\varepsilon_{\rm c})$ through the criterion given as

$$E_{\rm s}>\sqrt{2}\varepsilon_{\rm c}, \quad (6)$$

where the critical breaking strain is multiplied by $\sqrt{2}$ to be transformed to the critical significant strain amplitude. If the criterion is met, the ice floe would break up because of the strain failure (Williams et al., 2013a, b). Equation (6) is suitable for the narrow wave spectrum as the ideal cases in Section 3.2 (Williams et al., 2013a). The way to calculate critical ice breaking strain $\varepsilon_{\rm c}$ can be found in Williams et al. (2013a).

In the approach presented in this study, $E_{\rm s}$ is derived from the two-dimensional wave spectrum. Following Zhang et al. (2020), we assums that the ice breakup event occurs in the direction of the highest wave energy $(\theta_{\rm m})$ and only the wave energy within direction segment $|\theta_{\rm m}-\theta|\leqslant\frac{\pi}{2}$ contributes to the ice breakup, and then, $E_{\rm s}$ can be calculated as

$$E_{\rm s}=2\sqrt{\int_{\theta_{\rm m}-\frac{\pi}{2}}^{\theta_{\rm m}+\frac{\pi}{2}}\int_{0.04}^{1}S(\omega,\theta)\cos(\theta_{\rm m}-\theta)\left(\frac{h}{2}k_{\rm ice}^3\frac{|\Gamma_{\rm s}|}{k}\right)^2{\rm d}\omega{\rm d}\theta}, \quad (7)$$

where $h$ is the thickness of the ice floe, $\Gamma_{\rm s}$ is the transmission coefficient, $\omega$ is the angular frequency, $k$ is the wave number, and $k_{\rm ice}$ is the wave number of the ice plate, which is taken as the positive real root of Eq. (A.7) in Williams et al. (2013a).

#### 2.3.2 *Stress failure*

In the context of global warming and Arctic amplification, the Arctic sea ice becomes more fragile and less elastic, due to the increasing porosity and change of the crystal structure (Ivanov et al., 2016). In addition, the ice tends to be more rigid, and the ice floe breakup is caused by the flexural stress failure. The criterion of the stress failure is derived by comparing the critical flexural stress $(\sigma_{\rm c})$ and the maximum flexural stress $(\sigma_{\rm max})$ in the ice floe. Assuming the ice floe as a cube with rectangle cross-section and with the length, width and height as $l$, $b$, and $h$, respectively, then, based on the mechanics of materials, the flexural stress at any cross-section is calculated as

$$\sigma_{\rm CS}=\frac{My}{I_z}, \quad (8)$$

where $M$ is the bending moment, $y$ is the distance to the neutral axis at the vertical direction, and $I_z$ is the inertia moment, which for a rectangle cross-section is calculated as $I_z=\frac{1}{12}bh^3$. At a cross-section, the maximum flexural occurs at the top or the bottom, in which $y=\frac{1}{2}h$ or $-\frac{1}{2}h$. Thus,

$$\sigma_{\rm max}=\frac{M\frac{1}{12}h}{I_z}=\frac{M}{\frac{1}{6}bh^2}. \quad (9)$$

The bending moment is calculated by taking integral of all the vertical forces caused by passing waves, including the sea water buoyancy and the ice gravity. Note that the wave profile is assumed to be a sine function. If the width of the ice floe can be neglected, the bending moment is simply caused by the sea water buoyancy when the sea water particles are higher than the free sea surface. Meanwhile, when sea water particles are pulled down below the free sea surface, the bending moment is caused by the ice gravity. In short, if the width of the ice floe is ignored, the bending moment is derived from the relative potential energy.

When the width of the ice floe is not negligible, waves travel under the ice floe, and the water surface is limited by the bottom surface of the ice. However, for the purpose of forming the imaginary regular wave profile, the water particles are assumed to be driven by the moving wave energy. In addition, the kinetic energy of the water particles is not converted to the potential energy of the wave profile, but this energy, which could move the water particles above or under the free sea surface, is partially converted to the pressure normal to the ice bottom surface. This pressure is equal to a portion of the buoyancy of the water above

the sea surface and the gravity of the ice below the sea surface, as if the imaginary wave profile exists when the ice floe is an elastic material. In this study, it is assumed that the contribution of the wave potential energy to the ice floe bending momentum is $\Gamma_f$. In support of the assumptions taken in this study, Meylan et al. (2015) has established experimental and theoretical models to study the flexure of the plastic floe induced by passing waves, in which the floe's flexural motion is nearly uniform along the cross-section.

In this study, the ice density $(\rho_i)$ and the water density $(\rho_w)$ are assumed equal so that the bending moment can be calculated based on the wave profile. The force analysis (Fig. 1) shows that the horizontal red line is the free sea surface located below the top surface of the ice floe at $0.1h$, in which $h$ is the thickness of the ice floe. A Cartesian coordinate system is assumed that the $x$ coordinate is located at the free sea surface and the $y$ coordinate is located at the left side of the floe.

Since the density of the water and ice are assumed equal, the sum of the sea water buoyancy above the free sea surface (green vectors in Fig. 1) and the sum of the ice gravity below the free sea surface (red vectors in Fig. 1) are balanced. However the distribution of forces could lead to bending moment at the cross-section. It can be easily proved that the maximum bending moment occurs at the wave crest or the wave trough, which has the same magnitude. Therefore, the bending moment at the wave crest, cross-section C, is calculated. The bending moment at the cross-section C caused by the vertical force between the cross-section A and B is

$$M_C^{A-B} = \int_0^{\lambda} \rho g A \Gamma_f \sin\left(kx - \frac{\pi}{2}\right)\left(\frac{3}{2}\lambda - x\right) dx, \tag{10}$$

where $\rho = \rho_i = \rho_w$, and $M_C^{A-B}$ equals zero. Thus, if the floe diameter is assumed to be much larger than the wave length, there are always multiple integrals of wave lengths acting on the ice floe. In addition, the bending moment at any wave crest caused by the wave induced vertical force beyond the distance of $\lambda/2$ is integrally zero. The bending moment at the cross-section C is totally induced by the vertical force within one wave length, from cross-section B to D, in which the bending moment is

$$M_C^{B-D}{}_1 = 2 \times \int_0^{\frac{\lambda}{2}} \rho g A \Gamma_f \sin\left(kx - \frac{\pi}{2}\right)\left(x - \frac{\lambda}{2}\right) dx = \frac{\rho g A \lambda^2}{\pi^2}. \tag{11}$$

This estimation is reasonable when the wave crest is lower than the top surface of the ice floe (Fig. 1a). When the wave height is higher than $0.1h$, the wave crest will be above the ice surface and the force analysis between cross-section B and D is shown in Fig. 1b. In Fig. 1b, the buoyancy over the free surface and the ice gravity below the free surface are not equal because of the wave overwashing. Thus, the bending moment at the cross-section C should be reconsidered.

The ice floe in Fig. 1b has a trend to become stable. Note that

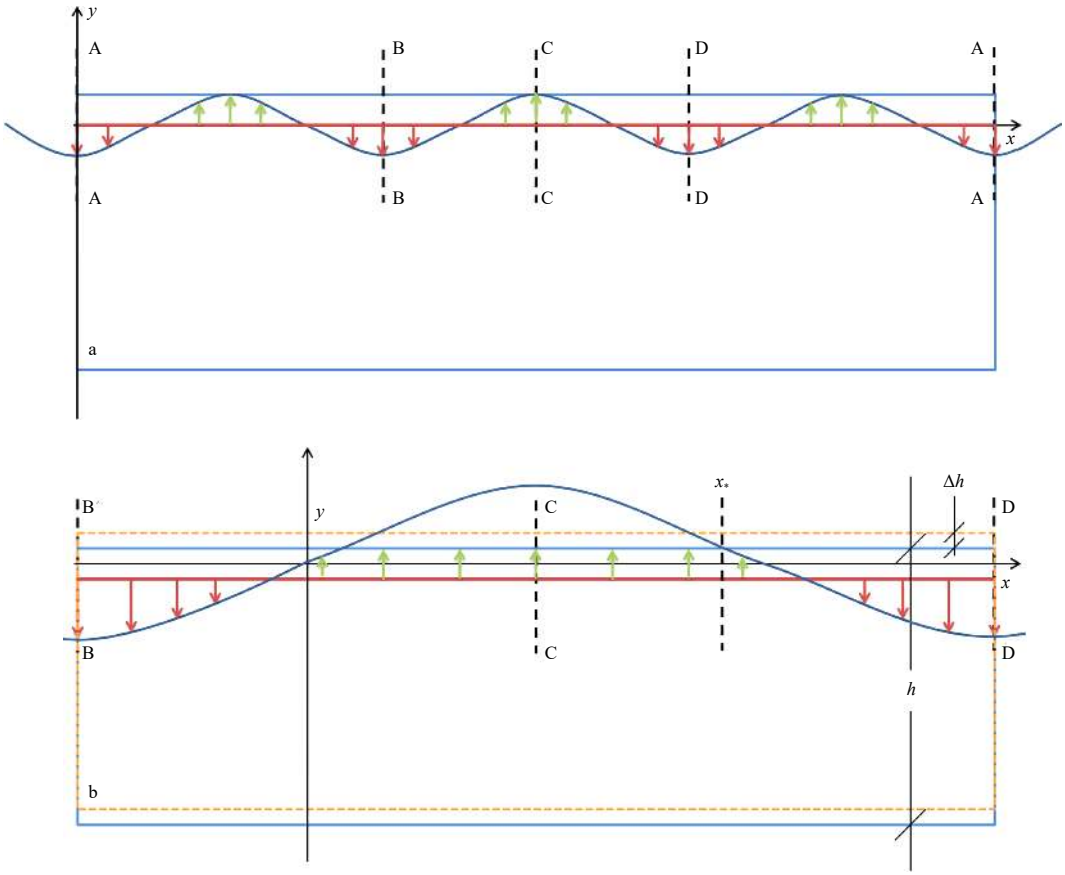


**Fig. 1.** The force analysis of an ice floe when wave traveling through. Wave crests are lower than the ice floe surface and stay stable (a), and wave crests are over the ice floe surface and ice floe sink to become stable again (b). The red lines are free surfaces. The orange imaginary rectangles are original floe position when it is still unstable. Green vectors are buoyance over free surface while red vectors are ice gravity below free surface.

the orange dashed rectangle is the original status, which should decline by a distance of $\Delta h$ to balance the wave-induced buoyancy above the free surface and the gravity below the free surface. The blue rectangle is the final status. The $x$ component of the intersection of the ice floe surface and sea surface within the section C-D is $x_*$, which is related to $\Delta h$ as follows:

$$A\sin(kx_*) = 0.1h - \Delta h. \tag{12}$$

In section C–D, there is only one solution to Eq. (12), which is

$$x_* = \left[\frac{\pi}{2} - \sin^{-1}\left(\frac{0.1h - \Delta h}{A}\right)\right]/k. \tag{13}$$

When the ice floes become stable again, the buoyancy above $0.1h$ caused by the wave and the floe self-gravity below should be the same. Thus,

$$\left(x_* - \frac{\lambda}{4}\right)0.1h + \int_{x_*}^{\frac{3}{4}\lambda}[A\sin(kx) + \Delta h]\,\mathrm{d}x = 0, \tag{14}$$

which yields

$$(0.1h - 3\Delta h)\frac{\lambda}{4} - (0.1h - \Delta h)x_* - \frac{A}{k}\cos(kx_*) = 0. \tag{15}$$

Thus, $x_*$ and $\Delta h$ can be derived by Eqs (13) and (15). Then, the bending moment at cross-section C is

$$\begin{aligned}\frac{1}{2}M_{\mathrm{C}}^{\mathrm{B-D}}{}_2 = M_{\mathrm{C}}^{\mathrm{C-D}}{}_2 = &\int_{\frac{\lambda}{4}}^{x_*}\rho g(0.1h)\,\Gamma_{\mathrm{f}}\left(\frac{3}{4}\lambda - x\right)\mathrm{d}x + \\ &\int_{x_*}^{\frac{3}{4}\lambda}\rho g[A\sin(kx) + \Delta h]\,\Gamma_{\mathrm{f}}\left(\frac{3}{4}\lambda - x\right)\mathrm{d}x,\end{aligned} \tag{16}$$

and

$$\begin{aligned}M_{\mathrm{C}}^{\mathrm{B-D}}{}_2 = &2\rho g\Gamma_{\mathrm{f}}\left\{0.1h\left(\frac{3}{4}\lambda x_* - \frac{1}{2}x_*^2 - \frac{5}{32}\lambda^2\right) + \right. \\ &A\left[\frac{1}{k^2} + \frac{1}{k^2}\sin(kx_*) - \frac{1}{k}x_*\cos(kx_*) + \frac{3\lambda}{4k}\cos(kx_*)\right] + \\ &\left.\left(\frac{9}{32}\Delta h\lambda^2 + \frac{\Delta h}{2}x_*^2 - \frac{3}{4}\lambda\Delta h x_*\right)\right\}.\end{aligned} \tag{17}$$

Thus, the maximum flexural stress is $\sigma_{\max} = \dfrac{M_{\mathrm{C}}^{\mathrm{B-D}}}{\frac{1}{6}bh^2}$, in which $M_{\mathrm{C}}^{\mathrm{B-D}}$ equals $M_{\mathrm{C}}^{\mathrm{B-D}}{}_1$ if the wave profile does not cross the ice floe surface, and when the wave crest is higher than the ice floe surface, $M_{\mathrm{C}}^{\mathrm{B-D}}$ should be $M_{\mathrm{C}}^{\mathrm{B-D}}{}_2$. Thus,

$$M_{\mathrm{C}}^{\mathrm{B-D}} = \begin{cases}\dfrac{\rho g A\lambda^2}{\pi^2}, & A \leqslant 0.1h, \\ 2\rho g\Gamma_{\mathrm{f}}\left\{0.1h\left(\frac{3}{4}\lambda x_* - \frac{1}{2}x_*^2 - \frac{5}{32}\lambda^2\right) + \right. \\ A\left[\frac{1}{k^2} + \frac{1}{k^2}\sin(kx_*) - \frac{1}{k}x_*\cos(kx_*) + \frac{3\lambda}{4k}\cos(kx_*)\right] + \\ \left.\left(\frac{9}{32}\Delta h\lambda^2 + \frac{\Delta h}{2}x_*^2 - \frac{3}{4}\lambda\Delta h x_*\right)\right\}, & A > 0.1h.\end{cases} \tag{18}$$

Note that the stress failure is reached, and the ice breakup happens when $\sigma_{\max} > \sigma_{\mathrm{c}}$, in which $\sigma_{\mathrm{c}}$ can be found in Zhang et al. (2020).

## 3 Results

### 3.1 *The strain and stress yield critical wave amplitude*

The critical wave amplitude $(A_{\mathrm{c}})$ can be given by both strain $(\varepsilon_{\mathrm{c}})$ and stress $(\sigma_{\mathrm{c}})$ yield limits. If only the strain-induced ice breakup is considered, the possibility of the ice breakup caused by small amplitude long wave may be remarkably underestimated. One example is the ice breakup events observed during the SIPEX-2 voyage in the Aurora Australia. In the deeper ice-covered sea, ice breakup events were also observed 455 km and 502 km away from the ice edge, and the wave amplitudes were only about 0.1 m. These two breakup events were not well reproduced by the simple strain failure model, even though the significant wave height was overestimated (Kohout et al., 2015). Thus, the simple model defining breakup in terms of the strain is proved to be insufficient (Kohout et al., 2015).

The strain and stress yield critical significant wave height $(\mathrm{SWH_c})$ is shown in Fig. 2. The ratio of the kinetic energy transformed to the ice-bottom pressure $(\Gamma_{\mathrm{f}})$ is set to 0.1 and $\Gamma_{\mathrm{s}}$ is assumed to be 1. The critical wave amplitudes for the ice thicknesses of 1 m, 2 m and 3 m are separately shown. The red, green and blue lines refer to the $\mathrm{SWH_c}$ calculated from the critical strain, $M_{\mathrm{C}}^{\mathrm{B-D}}{}_1$ induced the critical stress, which is calculated by the combination of $M_{\mathrm{C}}^{\mathrm{B-D}}{}_1$ and $M_{\mathrm{C}}^{\mathrm{B-D}}{}_2$. The solid lines refer to the relatively small $\mathrm{SWH_c}$, comparing the strain and stress yield amplitudes, while the dashed lines are relatively large and were abandoned.

By comparing Figs 2a, b and c, it is noticed that the ice floes would be more difficult to be broken if they become thicker. The strain failure is more important if the ice floes become thicker, which is embodied by the increasing transfer peak period (Tpeak) from the strain failure to the stress failure with increasing ice thickness. The tendencies of the yield amplitudes with different ice thicknesses are similar. Thus, only Fig. 2a will be described in the following paragraph.

When Tpeak is less than 6.9 s, the ice breakup is triggered by the wave-induced strain. The yield amplitude is 0.318 m when Tpeak is 2.5 s and decreased with increasing Tpeak until Tpeak = 5.4 s and the lowest $\mathrm{SWH_c}$ is 0.233 m. Then, it increases with increasing Tpeak and reaches 0.243 m when Tpeak = 7.1 s. When Tpeak is larger than 7.1 s, the stress failure controls the ice breakup. When waves become longer, $\mathrm{SWH_c}$ rapidly decreases until Tpeak = 15 s, and eventually drops from 0.243 m to 0.008 m. The transfer Tpeak would become small if $M_{\mathrm{C}}^{\mathrm{B-D}}{}_2$ is not considered and it drops from 7.1 s to 6.3 s. Moreover, Fig. 2 shows that if the stress yield is not considered, yield SWH increases with the increasing wave peak period, when Tpeak is larger than 5.4 s. When Tpeak = 15 s, the yield amplitude can be 0.63 m. However, the real situation is that the bending momentum in ice floe keeps increasing when Tpeak increases from 7.1 s to 15 s. Thus, the $\mathrm{SWH_c}$ drops monotonously to a small value. For the cases, in which the ice thickness is 2 m and 3 m, the $\mathrm{SWH_c}$ is 0.03 m and 0.067 m, respectively, when Tpeak = 15 s.

### 3.2 *Application to the SIPEX-2 voyage*

There are three floe breakup events during the SIPEX-2 voyage in the Aurora Australia. One event occurs at 00:00 on October 9, 2012 Coordinated Universal Time (UTC), for which there is no accurate SWH and Tpeak data. Thus, the focus is on the other two floe breakup events (Table 1). If the strain failure is the only

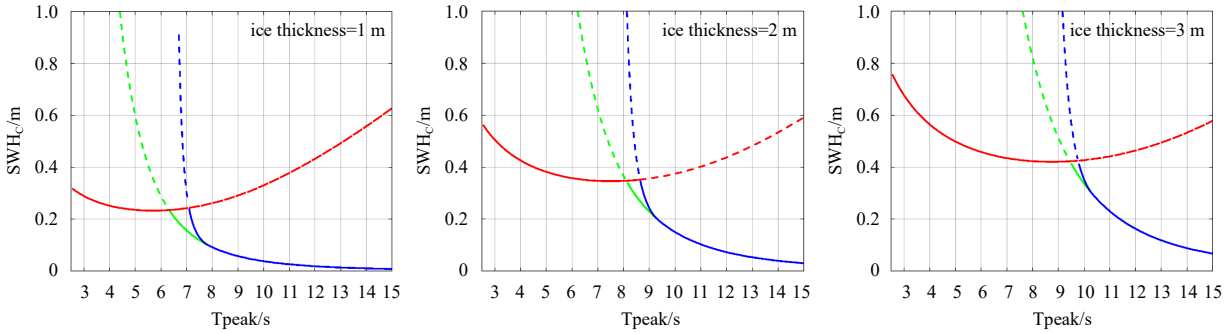


**Fig. 2.** Changes of the critical significant wave height (SWH$_c$) versus peak period (Tpeak) when ice thickness is 1 m (a), 2 m (b), and 3 m (c). The red, green and blue lines refer to the critical SWH calculated from the critical strain, $M_C^{B-D}{}_1$ induced critical stress and critical stress calculated from the combination of $M_C^{B-D}{}_1$ and $M_C^{B-D}{}_2$. The solid lines refer to the relatively small critical wave amplitude, comparing the strain and stress yield amplitudes, while the imaginary lines are relatively large ones.

**Table 1.** An overview of the two ice floe breakup events, showing the time the events occur, the distances from the ice edge ($D$), the estimated observed SWH (SWH$_o$), Tpeak (Tpeak$_o$), the simulated SWH (SWH$_s$), and Tpeak (Tpeak$_s$)

| | Time | $D$/km | SWH$_o$/m | SWH$_s$/m | Tpeak$_o$/s | Tpeak$_s$/s |
|---|---|---|---|---|---|---|
| Event A | 09:00 Sept. 25, 2012 | 244 | 0.5 | 0.37 | 15 | 15.4 |
| Event B | 13:00 Oct. 1, 2012 | 455 | 0.1 | 0.29 | 15 | 15.4 |

trigger of the ice floe breakup, which was 455 km from the ice edge deep in the ice sea, according to the observed significant wave height, the ice floe breakup was not supposed to be observed at 13:00 on October 1, 2012 (UTC) (Kohout et al., 2015). In addition, even though the significant wave heights were obviously overestimated by the numerical model, the strain model still could not predict the occurrence of the ice breakups (Kohout et al., 2015).

An ideal model is established to simulate the wave-ice interaction during the SIPEX-2 voyage. The model was run with an optional setting of 'wave-only' of FVCOM. Thus the current velocity was constantly zero, and the wave model was not influenced by temperature and salinity. For the purpose of fully testing the interaction between the ice and wave, and avoiding the errors due to solid boundary, the horizontal mesh grid is designed as a circular partially ice-covered sea, with the latitudes from 78°S to 90°S (Fig. 3a), and the depth was set to 1 km to avoid wave deformations in shallow water. The Antarctic continent was not included in the ideal model for simplification, as it did not influence model results when waves were from low latitudes and the integration time was short. The horizontal resolution of the mesh grid is regularly designed to be around 10 km, and the design of the mesh grid is the typical FVCOM triangle grid. Note that the perimeter of the circular sea is an open boundary, and the model integration time step is 20 s.

Waves with constant significant wave height and peak frequency, which follow the Joint North Sea Wave Project (JONSWAP) parameterization, keep traveling inside from the open boundary, in the normal direction. The ice is set to pre-cover the water surface, where latitude is higher than 80°S, and the ice concentration linearly increases from 0.8 to 1 when latitude increases from 80°S to 85°S, and it is constant, equal to 1, for latit-

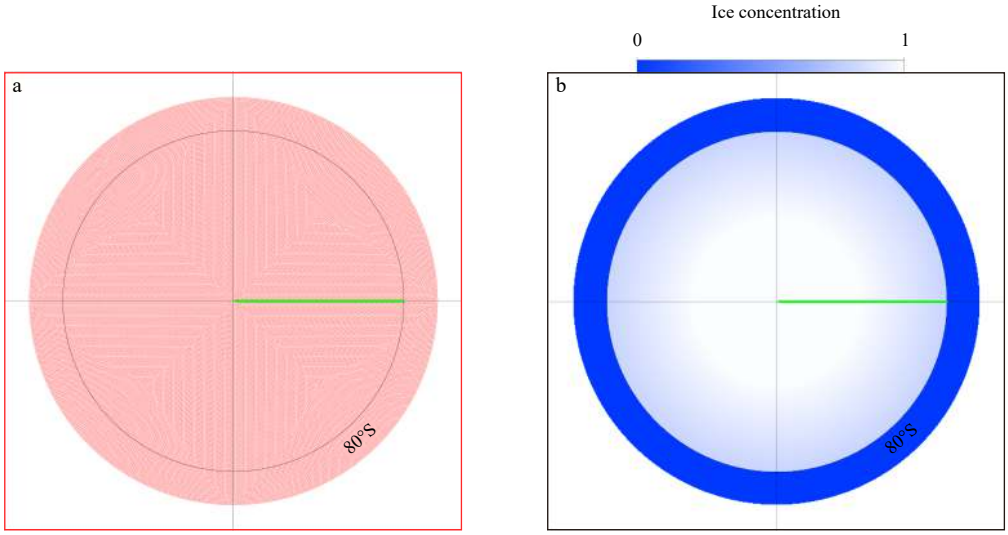


**Fig. 3.** The horizontal mesh grid of the ideal model (a) and the ice concentration (b). The green line is the transect which is show in Fig. 4.

udes higher than 85°S (Fig. 3b). According to Worby et al. (2011), the ice thickness is about 1 m near the ice edge and the fast ice is 2–3 m thick. Thus, in the ideal model, the ice thickness linearly increases from 1 m to 2.5 m as the latitude increases from 80°S to 85°S, and it is 2.5 m when latitude is higher than 85°S.

Four cases were set to study the waves in the MIZ and the possibility of the ice breakup (Table 2). In cases 1 and 2, the significant wave height and peak period at the open boundary are 2.2 m and 12 s, respectively, to reproduce the first floe breakup event described by Kohout et al. (2015). In cases 3 and 4, these variables are 5 m and 15 s, respectively, similar to the ice edge wave situation of the second floe breakup event described by Kohout et al. (2015). In cases 1 and 3, only the strain model (OM) is applied and in cases 2 and 4, both the stain and stress models (TM) are applied. In this study, the stress implemented in the stress model is based on the critical stress calculated from the combination of $M_C^{B-D}{}_1$ and $M_C^{B-D}{}_2$, because the SWH is over one-tenth of the ice thickness until it deepens in the ice-covered sea.

**Table 2.** Model setting for four cases

| | Open boundary | | Wave-induced ice yield scheme | |
|---|---|---|---|---|
| | SWH/m | Tpeak/s | Strain model | Stress model |
| Case 1 | 2.2 | 12 | √ | |
| Case 2 | 2.2 | 12 | √ | √ |
| Case 3 | 5 | 15 | √ | |
| Case 4 | 5 | 15 | √ | √ |

Due to the mesh grid, the ice field and the open boundary conditions are symmetrical so that the simulation results can be illustrated in one section from the ice edge to North Pole. Figure 4 shows the significant wave height, peak period, and floe diameter along this section. Twelve lines should be noticed in each plot, in which different colors represent the situations every 2 h.

Figure 4 shows the process that the wave energy penetrates the ice-covered sea. It is shown that the wave energy decays when the waves travel into the ice. As the wave period is longer, the wave energy can penetrate deeper into the ice-covered sea.

Based on the ice-induced wave attenuation model, the wave energy decreases when it encounters more ice floe. Note that if ice floes break, the number of ice floes waves encountered per unit distance increases and the wave attenuation coefficient increases. Thus, by comparing the final Tpeak of Figs 4a and c for the OM model and Figs 4b and d for the TM model, it is noticed that the wave energy with Tpeak = 15.4 s can penetrate deeper into the ice sea in the OM than the TM, which means that the wave attenuation is stronger in TM because of the ice floe breakup. Significant wave heights are totally the same in the area where both models predict the ice breakup. However, in the deep ice sea, wave energy is more rapidly attenuated by the ice, and signific-

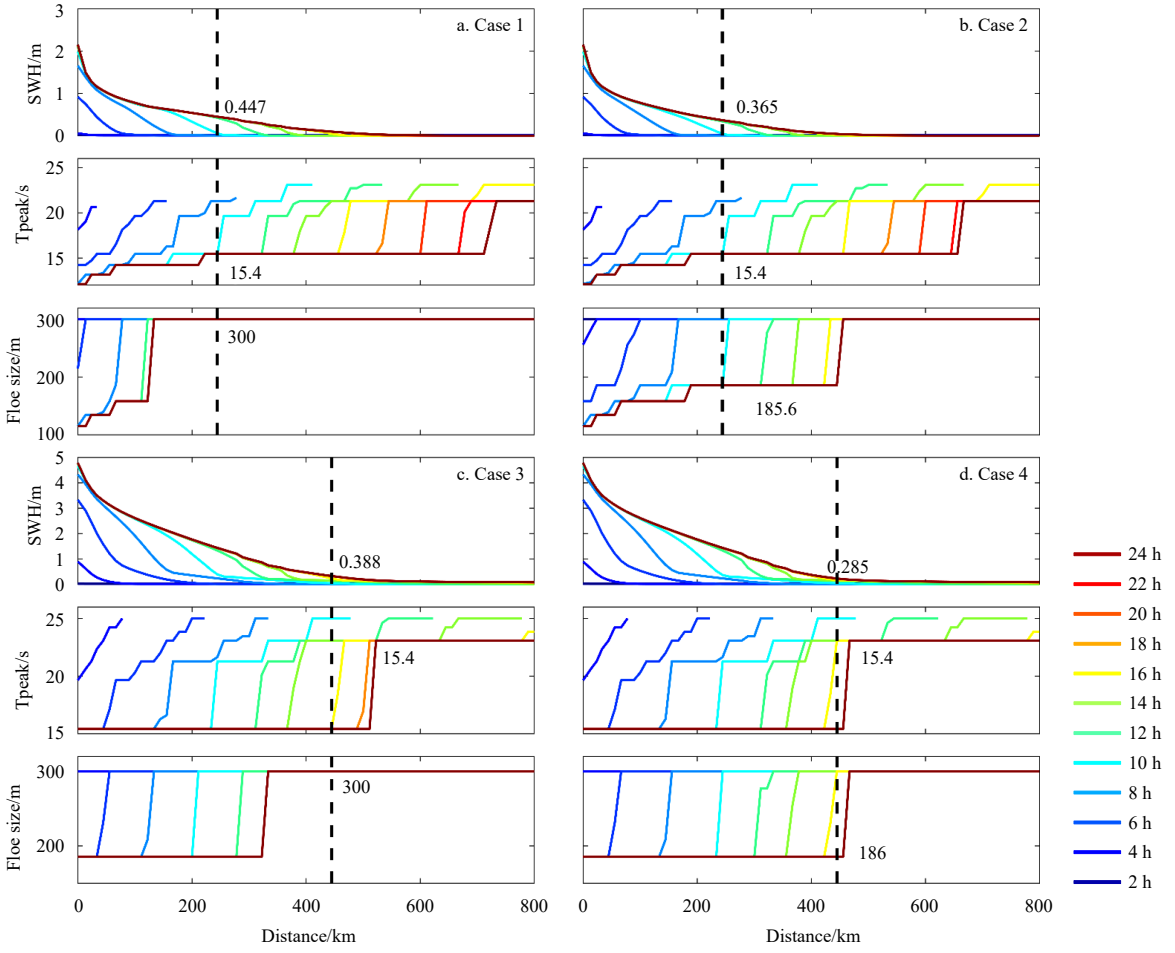


**Fig. 4.** Changes of the significant wave height (SWH), peak period (Tpeak) and floe size versus the distance from the ice edge, for Case 1 to Case 4. Different colors, from blue to red, refer to different times, with the time intervals of each adjacent line being 2 h. The numbers are the value at the black dashed line of the final situation.

ant wave heights are lower in cases 2 and 4 than in cases 1 and 3 because maximum ice floe sizes in cases 2 and 4 are smaller.

By comparing the final situations of cases 1 and 2, which are illustrated in Figs 4a and b, it could be noticed that the wave energy propagates with unapparent difference. The final Tpeak at the ice breakup location (the black dashed line) is similar in every case. However, due to more ice breakup events, the significant wave height at the black dashed line in Case 2 is smaller than in Case 1. In addition, the maximum floe sizes are distinctly different between these two cases. In Case 1, the maximum floe size is 114 m until the wave travels 22 km into the MIZ, and then it becomes 134.5 m until the wave travels 66 km, and it reaches 158 m in the depth of 133 km from the ice edge, as the ice floes do not break in the deeper ice-covered sea. In Case 2, before the wave travels 292 km from the ice edge, the maximum ice floe diameters are nearly the same as in Case 1, but the maximum floe size reaches 185.6 m in farther areas and the ice floe is possible to break until 489 km from the ice edge. Figures 4c and d show the simulation results when the significant wave height at the open boundary increases to 5 m, which corresponds to the situation of Event B. The final condition shows that peak periods are the same for both cases, but SWH for Case 4 is about 0.1 m lower than that in Case 3. In Case 3, the ice floe is able to break and reaches 185.6 m until 344 km away from the ice edge, while, in Case 4, the ice floe can break at the distance of 511 km. In contrast to cases 1 and 3, cases 2 and 4, which adopted both the strain and stress failure models, predicted the ice breakup events A and B successfully. As Table 1 shows, the numerical results and field data of SWHs and Tpeaks at the locations of the ice break up events are in good agreement. In summary, it can be concluded that the TM can better simulate the ice breakup event in the ice sea, and, in the meantime, it slightly influences the wave field in the ice sea.

It is known that the fraction of lateral melt ($R_{\mathrm{SID}}$) (Steele, 1992) is a function of vertically averaged lateral melt rate ($M_{\mathrm{a}}$) and the ice floe diameter ($D_{\mathrm{F}}$),

$$R_{\mathrm{SID}} = \left| \frac{M_{\mathrm{a}}\pi}{\alpha D_{\mathrm{F}}} \right|, \tag{19}$$

where $\alpha = 0.66$, and $M_{\mathrm{a}} = m_1(T_{\mathrm{w}} - T_{\mathrm{f}})^{m_2}$, in which $m_1 = 1.6\times 10^{-6}$ m/(s $\cdot$ deg$^{m_2}$), $m_2 = 1.36$, and $T_{\mathrm{w}}$ and $T_{\mathrm{f}}$ are the sea water and the floe temperature, respectively (Josberger and Martin, 1981; Maykut and Perovich, 1987). It is obvious that the lateral melt of the ice is directly controlled by the floe size. A decrease in the ice floe diameter due to the ice breakup can linearly increase the rate of the lateral melt, thus, accelerate the ice melt in both polar regions.

## 4 Conclusions

In this study, a fully coupled ice-wave dynamical model was implemented in FVCOM, to analyze the ice floe breakup events during the SIPEX-2 voyage. This model was established with two closely intertwined parts: the existing ice-induced wave attenuation scheme, and a wave-induced ice breakup scheme. For ice-induced wave attenuation, we adopted the design from Zhang et al. (2020). As the ice cannot be treated either as an ideal elastic material or a rigid body, both the strain and stress failures essentially can cause the ice breakup. We improved the stress failure scheme and adopted the theory of Williams et al. (2013a) for the strain failure scheme. The stress failure was controlled by the bending moment, which is the integral of the sea water buoyancy and the ice floe gravity forces. The stress failure was judged by comparing the critical flexure stress and the maximum flexure stress. In this paper, both strain and stress failures were taken as the criteria to estimate the possibility of the ice breakup.

The strain and stress yield critical significant wave heights were derived when the ice thicknesses were supposed to be 1 m, 2 m, and 3 m. The features of the three cases were similar so that the strain failure can cause the ice breakup at the high-frequency side, while the stress failure is the main reason for the ice breakup at the low-frequency side. Neglecting either of these two mechanisms results in underestimation of the possibility of the ice breakup. One good example is the observed ice breakups during the SIPEX-2 voyage in the Aurora Australia. In this paper, ideal cases were established to simulate the wave field in the ice-covered sea, referred to the boundary wave condition and the ice field during the SIPEX-2 voyage. The simulation results showed that the stress failure induced ice breakup could dramatically enhance the possibility of the ice breakup in the deep ice-covered sea, where the wave period was long and the wave height was low, on account of the ice-induced wave attenuation. The significant wave heights in the deep ice-covered sea were slightly reduced because of the ice breakup, which resulted in more ice floes encountering. The simulation results, which adopted both the strain and stress failure theories, matched appropriately with the observed ice breakup event and theoretically could explain the ice breakup in the deep ice-covered sea. By enhancing the simulation accuracy of the ice breakup events caused by waves, the ice extent in both polar areas can be better predicted.

***Acknowledgements***

We sincerely appreciate the data support from Kohout Alison from National Institute of Water and Atmospheric Research, New Zealand, who shared the data about three floe breakup events during the SIPEX-2 voyage in the Aurora Australia. This work was improved because of precious comments from two anonymous reviewers, and we are so grateful.

## References

Asplin M G, Galley R, Barber D G, et al. 2012. Fracture of summer perennial sea ice by ocean swell as a result of Arctic storms. Journal of Geophysical Research: Oceans, 117(C6): C06025

Bai Peng, Wang Jia, Chu P, et al. 2020. Modeling the ice-attenuated waves in the Great Lakes. Ocean Dynamics, 70(7): 991–1003, doi: 10.1007/s10236-020-01379-z

Cavalieri D J, Parkinson C L, Vinnikov K Y. 2003. 30-Year satellite record reveals contrasting Arctic and Antarctic decadal sea ice variability. Geophysical Research Letters, 30(18): 1970

Chen Changsheng, Beardsley R C, Cowles G. 2006. An unstructured grid, finite-volume coastal ocean model (FVCOM) system. Oceanography, 19(1): 78–89, doi: 10.5670/oceanog.2006.92

Chen C, Beardsley R C, Cowles G, et al. 2013. An unstructured-grid, finite-volume community ocean model FVCOM user manual. SMAST-UMASSD Technical Report-13-0701, Dartmouth: University of Massachusetts-Dartmouth, 404

Chen Changsheng, Liu Hedong, Beardsley R C. 2003. An unstructured grid, finite-volume, three-dimensional, primitive equations ocean model: application to coastal ocean and estuaries. Journal of Atmospheric and Oceanic Technology, 20(1): 159–186, doi: 10.1175/1520-0426(2003)020<0159:AUGFVT>2.0.CO;2

Dean C H. 1966. The attenuation of ocean waves near the open ocean/pack ice boundary. In: Proceedings of the Symposium on Antarctic Oceanography. Santiago, Chile: Scientific Committee on Antarctic Research, 13–16

Doble M J, Bidlot J R. 2013. Wave buoy measurements at the Antarctic sea ice edge compared with an enhanced ECMWF WAM:

progress towards global waves-in-ice modelling. Ocean Modelling, 70: 166–173, doi: 10.1016/j.ocemod.2013.05.012

Dumont D, Kohout A, Bertino L. 2011. A wave-based model for the marginal ice zone including a floe breaking parameterization. Journal of Geophysical Research: Oceans, 116(C4): C04001

Fujisaki-Manome A, Anderson E J, Kessler J A, et al. 2020. Simulating impacts of precipitation on ice cover and surface water temperature across large lakes. Journal of Geophysical Research: Oceans, 125(5): e2019JC015950, doi: 10.1029/2019JC015950

Gao Guoping, Chen Changsheng, Qi Jianhua, et al. 2011. An unstructured-grid, finite-volume sea ice model: development, validation, and application. Journal of Geophysical Research: Oceans, 116(C8): C00D04

Ivanov V, Alexeev V, Koldunov N V, et al. 2016. Arctic ocean heat impact on regional ice decay: a suggested positive feedback. Journal of Physical Oceanography, 46(5): 1437–1456, doi: 10.1175/JPO-D-15-0144.1

Josberger E G, Martin S. 1981. A laboratory and theoretical study of the boundary layer adjacent to a vertical melting ice wall in salt water. Journal of Fluid Mechanics, 111: 439–473, doi: 10.1017/S0022112081002450

Kohout A L, Meylan M H. 2008. An elastic plate model for wave attenuation and ice floe breaking in the marginal ice zone. Journal of Geophysical Research: Oceans, 113(C9): C09016, doi: 10.1029/2007JC004434

Kohout A L, Williams M J M, Dean S M, et al. 2014. Storm-induced sea-ice breakup and the implications for ice extent. Nature, 509(7502): 604–607, doi: 10.1038/nature13262

Kohout A L, Williams M J M, Toyota T, et al. 2015. In situ observations of wave-induced sea ice breakup. Deep-Sea Research Part II: Topical Studies in Oceanography, 131: 22–27, doi: 10.1016/j.dsr2.2015.06.010

Kwok R, Cunningham G F, Wensnahan M, et al. 2009. Thinning and volume loss of the Arctic Ocean sea ice cover: 2003–2008. Journal of Geophysical Research: Oceans, 114(C7): C07005, doi: 10.1029/2009JC005312

Liu A K, Holt B, Vachon P W. 1991. Wave propagation in the marginal ice zone: model predictions and comparisons with buoy and synthetic aperture radar data. Journal of Geophysical Research: Oceans, 96(C3): 4605–4621, doi: 10.1029/90JC02267

Maykut G A, Perovich D K. 1987. The role of shortwave radiation in the summer decay of a sea ice cover. Journal of Geophysical Research: Oceans, 92(C7): 7032–7044, doi: 10.1029/JC092iC07p07032

Meier W, Stroeve J, Fetterer F, et al. 2005. Reductions in Arctic sea ice cover no longer limited to summer. Eos, Transactions American Geophysical Union, 86(36): 326

Meylan M H, Bennetts L G, Cavaliere C, et al. 2015. Experimental and theoretical models of wave-induced flexure of a sea ice floe. Physics of Fluids, 27(4): 041704, doi: 10.1063/1.4916573

Qi Jianhua, Chen Changsheng, Beardsley R C, et al. 2009. An unstructured-grid finite-volume surface wave model (FVCOM-SWAVE): implementation, validations and applications. Ocean Modelling, 28(1–3): 153–166, doi: 10.1016/j.ocemod.2009.01.007

Robin G D Q. 1963. Wave propagation through fields of pack ice. Philosophical Transactions of the Royal Society A: Mathematical, Physical and Engineering Sciences, 255(1057): 313–339

Schwarz J, Frederking R, Gavrillo V, et al. 1981. Standardized testing methods for measuring mechanical properties of ice. Cold Regions Science and Technology, 4(3): 245–253, doi: 10.1016/0165-232X(81)90007-0

Squire V A. 2020. Ocean wave interactions with sea ice: a reappraisal. Annual Review of Fluid Mechanics, 52: 37–60, doi: 10.1146/annurev-fluid-010719-060301

Squire V A, Meylan M. 1994. Changes to ocean wave spectra in a marginal ice zone 2. Osaka, Japan: The International Society of Offshore and Polar Engineers

Squire V A. 2007. Of ocean waves and sea–ice revisited. Cold Regions Science and Technology, 49: 110–133, doi: 10.1016/j.coldregions.2007.04.007

Squire V A, Vaughan G L, Bennetts L G. 2009. Ocean surface wave evolvement in the Arctic Basin. Geophysical Research Letters, 36(22): L22502, doi: 10.1029/2009GL040676

Squire V A. 2020. Ocean wave interactions with sea ice: a reappraisal. Annual Review of Fluid Mechanics, 52(1): 37–60

Steele M. 1992. Sea ice melting and floe geometry in a simple ice-ocean model. Journal of Geophysical Research: Oceans, 97(C11): 17729–17738, doi: 10.1029/92JC01755

Stroeve J, Holland M M, Meier W, et al. 2007. Arctic sea ice decline: faster than forecast. Geophysical Research Letters, 34(9): L09501

Wadhams P, Squire V A, Goodman D J, et al. 1988. The attenuation rates of ocean waves in the marginal ice zone. Journal of Geophysical Research: Oceans, 93(C6): 6799–6818, doi: 10.1029/JC093iC06p06799

Williams T D, Bennetts L G, Squire V A, et al. 2013a. Wave-ice interactions in the marginal ice zone. Part 1: theoretical foundations. Ocean Modelling, 71: 81–91, doi: 10.1016/j.ocemod.2013.05.010

Williams T D, Bennetts L B, Squire V A, et al. 2013b. Wave-ice interactions in the marginal ice zone. Part 2: numerical implementation and sensitivity studies along 1D transects of the ocean surface. Ocean Modelling, 71: 92–101, doi: 10.1016/j.ocemod.2013.05.011

Worby A P, Steer A, Lieser J L, et al. 2011. Regional-scale sea-ice and snow thickness distributions from in situ and satellite measurements over East Antarctica during SIPEX 2007. Deep-Sea Research Part II: Topical Studies in Oceanography, 58(9–10): 1125–1136

Zhang Yang, Chen Changsheng, Beardsley R C, et al. 2020. Applications of an unstructured grid surface wave model (FVCOM-SWAVE) to the Arctic Ocean: the interaction between ocean waves and sea ice. Ocean Modelling, 145: 101532, doi: 10.1016/j.ocemod.2019.101532